Performance analysis of numerical schemes in highly swirling turbulent flows in cyclones

F. Kaya* and I. Karagoz

Uludag University, Mechanical Engineering Department, 16059, Gorukle Bursa, Turkey

The aim of this study is to investigate the suitability of various numerical schemes and turbulence models in highly complex swirling flows which occur in tangential inlet cyclones. Three-dimensional steady governing equations for incompressible turbulent flow inside a cyclone were solved numerically using Fluent CFD (computational fluid dynamics) code. The Reynolds stress turbulence model, the Standard k–ε and the RNG k–ε turbulence models together with various combinations of numerical schemes are used to obtain axial and tangential velocity profiles, pressure drop and turbulent quantities. Computational results were compared with experimental and numerical values given in the literature, so as to evaluate the performance of the numerical schemes and turbulent models. Comparison of CFD results with experimental data shows that the Reynolds Stress turbulence model yields a reasonably good prediction. Results obtained from the numerical tests have demonstrated that the use of the Presto interpolation scheme for pressure, the Simplec algorithm for pressure–velocity coupling and the quadratic upstream interpolation for convective kinetics (quick) scheme for momentum variables gives satisfactory results for highly swirling flows in cyclones.

Keywords: Cyclones, numerical schemes, swirling flows, turbulence models.

THE study of swirl flow is of technical and scientific interest because of its influence on transfer processes associated with recirculation flow field. One application of strongly swirling flow is cyclone separators which are widely used for various purposes, mainly for separating of dense phase in a multi-phase flow. Entrance of flow into a cyclone can be axial or tangential through the inlet section, which can be in different shapes for each cyclone. Cyclone separators operate under the action of centrifugal forces. Fluid mixture enters the cyclone and makes a swirling motion and, due to the centrifugal forces, the dense phase of the mixture gains a relative motion in the radial direction and is separated from the main flow. It is difficult to analyse this problem since, in addition to its 3D character, there are many parameters that influence this flow. The main performance characteristics of a cyclone separator are collection efficiency, fractional efficiencies and pressure losses. Many studies have been performed on this difficult problem for determination of these characteristics, but these studies are successful for only a certain range of Reynolds number and geometrical ratios. Therefore, developing more efficient cyclones have been essentially based on experiments rather than mathematical models[1–7]. The earlier models[8–11] are simple and include only a few parameters, but do not give satisfactory results.

A literature survey showed that the vortex length can be important for the prediction of collection efficiency, especially in short cyclones. But in long cyclones, the cyclone vortex may not reach the cone apex. The collection efficiency increases with increasing cyclone length up to a certain value and then starts decreasing (see, for example, Alexander[9] and Zhu and Lee[12]. The natural vortex length was first defined and formulated by Alexander[9]. In addition, Avci and Karagoz[13] proposed a theoretical model for prediction of cut-off size and collection efficiency as a function of geometrical and flow parameters, and fluid properties. This model extended to the modelling of pressure loses[14]. This model can be used satisfactorily for a wide range of geometry and flow conditions, as well as for optimization of some parameters depending on the operational conditions.

Computational fluid dynamics (CFD) has a great potential to predict the flow-field characteristics and particle trajectories inside the cyclone as well as the pressure drop[15]. The complicated swirling turbulent flow in a cyclone places great demands on the numerical techniques and turbulence models employed in the CFD codes when modelling the cyclone pressure drop and, axial and tangential velocities[16–18]. Although there are numerous computational works which use different numerical schemes in cyclone flow, none of them discusses the performances and errors erased from the numerical schemes.

In this study, the performance of various numerical techniques and interpolation schemes were investigated for the highly swirling flow inside a tangential inlet cyclone, by comparing the predicted results with the experimental and numerical values given in the literature[19]. Additionally, a comparison between two isotropic turbulence models, namely the Standard k–ε and the RNG k–ε turbulent model and the Reynolds stress model (RSM), which is an anisotropic turbulence model was made. Results obtained from the numerical tests have demonstrated that the key to the success of the CFD lies with the accurate description

*For correspondence. (e-mail: fkaya@uludag.edu.tr)

of the turbulent behaviour of the flow and adoption of relevant numerical techniques and interpolation schemes.

Governing equations and numerical solution

A cyclone separator consists of three main parts: the inlet, separation chamber and vortex finder. Tangential inlets are preferred for the separation of particles from gases[20]. Therefore, the Stairmand high-efficiency cyclone was used in this simulation (Figure 1). Its dimensions are given in Table 1.

The steady-state conservation of mass and momentum equations can be written in the following compact form[21]:

$$\frac{\partial(\rho u_j \phi)}{\partial x_j} = \frac{\partial}{\partial x_j}\left[\Gamma \frac{\partial \phi}{\partial x_j}\right] + S, \tag{1}$$

where ϕ is the general dependent variable, Γ the diffusivity which may be laminar or turbulent and S the source term. For the continuity equation, ϕ is 1, and Γ and S are zero. For the momentum equations, $\phi = u_i$, $\Gamma = \mu_{\text{eff}} = \mu + \mu_t$ and $S = -\partial P/\partial x_i + \rho g_i$. Reynolds stresses are given by:

$$-\rho\overline{u_i' u_j'} = \mu_t\left(\frac{\partial u_i}{\partial x_j} + \frac{\partial u_j}{\partial x_i}\right) - \frac{2}{3}\rho\delta_{ij}k. \tag{2}$$

The turbulent viscosity μ_t can be computed by combining the turbulent kinetic energy k and its dissipation rate ε as follows:

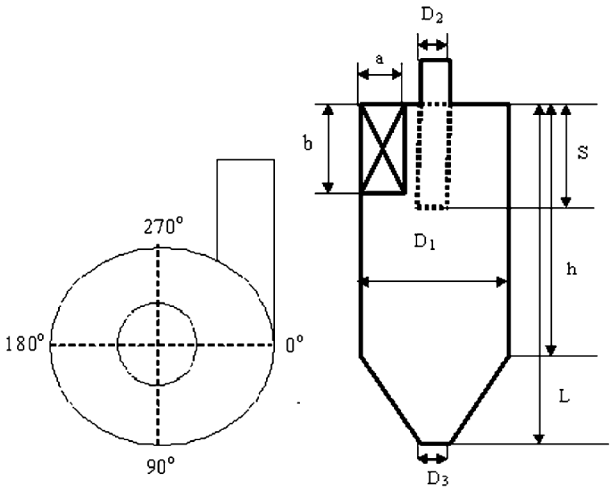

Figure 1. Tangential inlet cyclone.

Table 1. Cyclone geometry used in the present simulation

a (mm)	b (mm)	D_2 (mm)	S (mm)	h (mm)	L (mm)	D_3 (mm)	D_1 (mm)
32	85	85	85	255	680	32	170

$$\mu_t = C_\mu \rho \frac{k^2}{\varepsilon}. \tag{3}$$

Transport equations for k and ε in the RNG k–ε model, which is derived from Navier–Stokes equations using the renormalization group theory[22] can be written as:

$$\rho\frac{Dk}{Dt} = \frac{\partial}{\partial x_i}\left(\alpha_k \mu_{\text{eff}} \frac{\partial k}{\partial x_i}\right) + G_k - \rho\varepsilon, \tag{4}$$

and

$$\rho\frac{D\varepsilon}{Dt} = \frac{\partial}{\partial x_i}\left(\alpha_k \mu_{\text{eff}} \frac{\partial k}{\partial x_i}\right) + C_{1\varepsilon}\frac{\varepsilon}{k}G_k - C_{2\varepsilon}\rho\frac{\varepsilon^2}{k} - R. \tag{5}$$

Unlike the standard k–ε model, this model includes an analytical expression in addition to having an extra term R in the second equation. The model constants are assumed to have the following values: $C_{1\varepsilon} = 1.42$, $C_{2\varepsilon} = 1.68$ and $C_\mu = 0.0845$. Calculation of the terms can be found in the related literature.

Governing equations were solved numerically using finite volume-based Fluent CFD code. According to the basic idea of the control volume method, the computation domain is divided into a number of cells, and the differential equation is integrated over each cell to obtain the corresponding discretized equations. These algebraic equations were solved iteratively to obtain the field distribution of dependent variables. Different numerical schemes and various combinations of them have been used in the solutions and they are summarized in Table 2. Details on these schemes can be found in the literature. Due to difficulty to reach the convergence in simulations, the first order upwind scheme was applied for discretization of the Reynolds stresses.

The numerical calculation was made with a numerical grid as shown in Figure 2. Different grades of grid refinement were tested, with the first grid point located in various regions of the boundary layer. The grid refinement study shows that a total number of about 170,000 elements is sufficient to obtain a grid-independent solution, and further mesh refinement yields only small, insignificant changes in the numerical solution.

The boundary condition for air-flow velocities at the cyclone inlet was assumed to be uniform at 14.8 m/s. The outflow boundary condition was used at the exit. At the walls, no slip boundary condition was applied for velocity, and near-wall treatment was achieved using the standard and non-equilibrium wall functions.

Results and discussion

Strongly swirling turbulent flow inside a tangential inlet cyclone was solved numerically using Fluent CFD code,

Table 2. Methods used in the numerical solutions

	Numerical solution 2 (ns2)	Numerical solution 4 (ns4)	Numerical solution 5 (ns5)	Numerical solution 6 (ns6)	Numerical solution 8 (ns8)
Pressure	Presto	Presto	Presto	Presto	Second order
Pressure–velocity coupling	Simplec	Simplec	Simplec	Simplec	Simplec
Momentum	Second order	Quick	Second order	Quick	Second order
Turbulence kinetic energy	Second order	Second order	Second order	Quick	Second order
Turbulence dissipation rate	Second order	Second order	Second order	Quick	Second order
Reynolds stress	First order	First order	First order	First order	First order

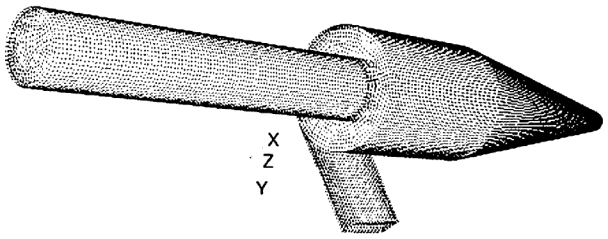

Figure 2. CFD surface mesh for the cyclone.

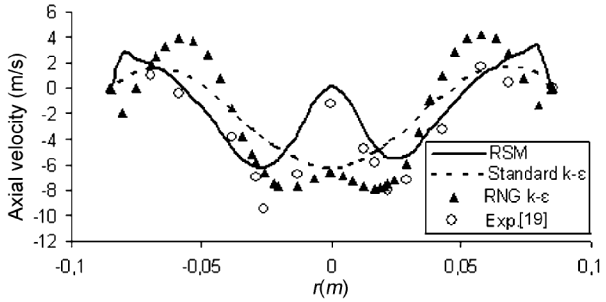

Figure 3. Comparison between computed axial velocity profiles and experimental data (z = 0.15 m, 90°–270°).

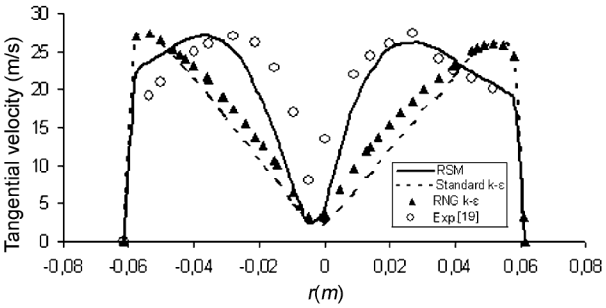

Figure 4. Comparison between computed tangential velocity profiles and experimental data (z = 0.4 m, 0°–180°)

with three different turbulence models, the RSM turbulence model, the Standard k–ε and the RNG k–ε turbulence models, with nonequilibrium wall function. Different numerical schemes were tested to obtain axial and tangential velocity profiles, pressure drop and turbulent quantities. The numerical results were compared with the experimental and numerical values given in the literature[19]. Table 2 shows the numerical schemes and algorithms tested in this study with the RSM turbulence model.

Comparison of turbulence models

Comparison of axial and tangential velocity profiles computed using three turbulence models with experimental data by Gong and Wang[19] is given in Figures 3 and 4, at different axial positions z, below the top of the cylindrical cyclone. Zero on the radial axis characterizes the centre of the cyclone. As can be seen, the RSM turbulence model performs much better compared to the other turbulence models. Although the tendency and behaviour of the computed velocity profiles are consistent with the experimental data, there are some discrepancies, especially in the core region in the comparison between measured velocities from the literature and the RSM predictions. Since this swirling flow is strongly affected by the flow and geometric conditions, and it is difficult to measure velocities precisely in such a complex flow, it is possible to conclude that these discrepancies are due to not only the turbulence model and numerical methods, but also experimental and measurement errors. The highly rotating fluid flow generates a strong anisotropy in the turbulent structure, and this causes the standard k–ε and the RNG k–ε turbulence models to provide inaccurate prediction of the fluid flow. Although the RNG k–ε model gives slightly better results compared to the Standard k–ε model, due to its swirl factor, it fails to produce Rankin-type tangential velocity distributions (Figure 4). Additionally, the standard k–ε and the RNG k–ε turbulence models under predict the pressure drop. However, the best prediction of the pressure drop is obtained by the RSM model as 1407 Pa.

Comparison of numerical schemes for pressure solutions

Presence of high-pressure gradients and double-vortex flow structure requires an efficient algorithm for the pressure computations. The presto pressure interpolation scheme is successful in this respect. High-order scheme for the flow parameters together with the presto algorithm

give better prediction of experimental data. Pressure drop values obtained from numerical tests are compared with experimental data in Table 3. Among the numerical solutions with the presto scheme, the best results for pressure drop are obtained with numerical solution 4 (ns4), which uses the Simplec algorithm for pressure–velocity coupling and the quick scheme for momentum equation. Although the first-order upwind schemes yield better convergence, they generally lead to inaccurate results. Therefore the quick scheme may be preferred in calculating momentum, turbulent kinetic energy and its dissipation rate equations. The quick interpolation scheme also helps minimize any artificial viscosity which may be introduced into the discretized form of the governing equations. Pressure contours in the vertical mid-plane of the cyclone are given in Figure 5. ns8 is considerably different from the others, especially in the core region, in terms of pressure magnitude and spiral shape of the low-pressure region in the centre.

Comparison of velocity fields

Comparison of velocity vectors obtained with ns2, ns8 and ns4 is given in Figure 6, in the mid-plane of the cyclone. Similar to Figure 5, ns8 presents a different velocity field, especially in the conical part. ns2 and ns4 give a complex flow field in which flow velocity increases towards the cone apex due to acceleration, and spiral-shaped inner vortex. Therefore, the presto scheme is able to reproduce the pressure field, and consequently a more accurate velocity field.

Comparison of axial velocity profiles predicted by five numerical solutions and experimental data[19] is given in Figure 7, at the axial position of z = 0.15 m, below the top

Table 3. Comparison between computed and experimental pressure drop (Pa)

ns2	ns4	ns5	ns6	ns8	Experimental[19]
1301	1407	1359	1393	890	1465.2

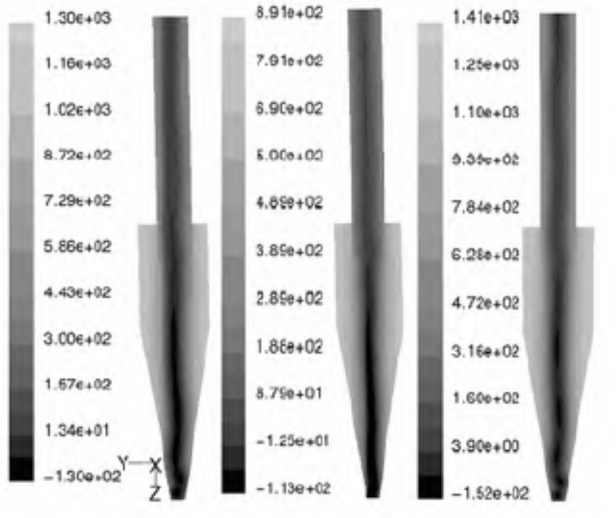

Figure 5. Contours of static pressure obtained with ns2, ns8 and ns4 respectively.

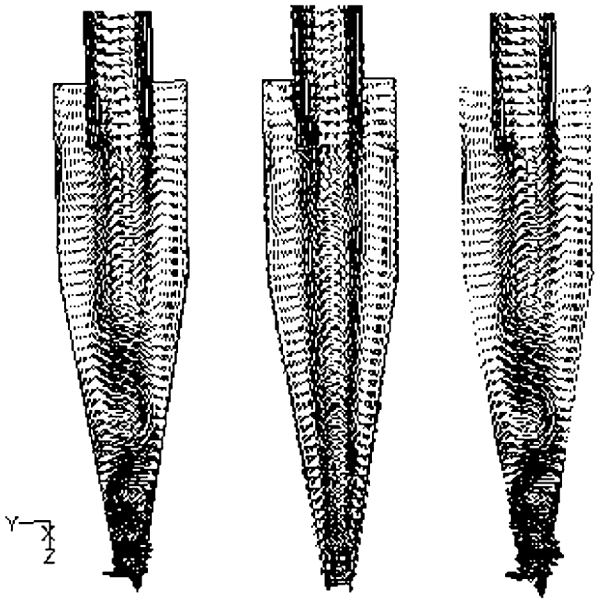

Figure 6. Mid-plane velocity vectors obtained with ns2, ns8 and ns4 respectively.

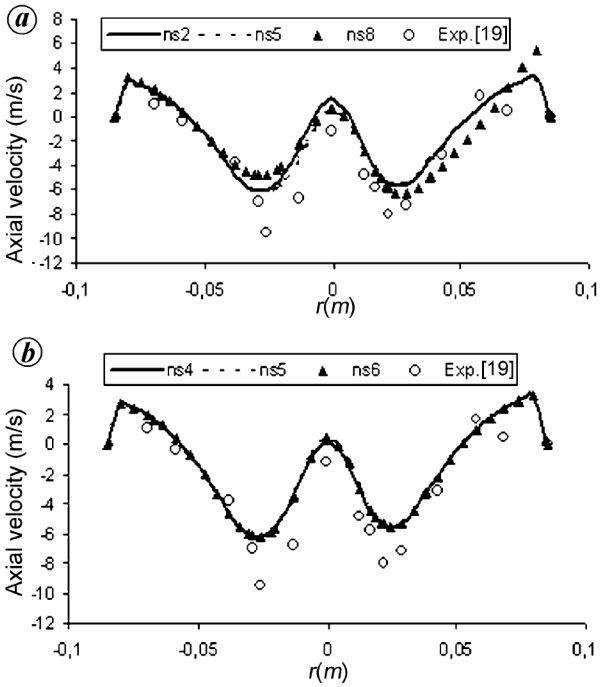

Figure 7 ***a***, ***b***. Comparison between computed axial velocity profiles and experimental data (z = 0.15 m, 90°–270°).

of the cylindrical cyclone body. Negative velocities are directed upward towards the outlet. There is an outer region close to the wall of the cyclone where the flow is directed downwards. The axial velocity displays a two-peak distribution in the interior up-flow region. The axial velocity gradually decreases towards the centre to a minimum, which may even be negative in some axial positions. At about two-third of the cyclone radius, the flow reverses. Although the numerical solutions under predict the maximum velocities in the core region, it is well confirmed that the numerical techniques used give reasonable results in agreement with the experimental data. Differences between the numerical predictions are close to each other, except for ns8.

Figure 8 gives a comparison between numerical predictions and experimental observations of tangential velocities at the axial position of $z = 0.4$ m from the top of the cyclone. The flow field in the cyclone indicates Rankin-type vortex, which is a combination of forced and free vortices, and well predicted by numerical simulations with the RSM turbulence model. Moreover, the axis of the vortex does not coincide with the axis of the geometry of the cyclone due to asymmetric location of one inlet pipe. In the central region where the flow rotates like a solid body because of forced vortex, the tangential velocity increases with increasing radius. The maximum computed tangential velocity of approximately 1.82 times the inlet velocity is reached at about half of the radius. As can be seen from Figure 8, the location of the maximum tangential velocity is over predicted by the simulation. Differences between the numerical predictions are also indistinguishable, except for ns8, which under predicts the tangential velocity profiles and gives maximum tangential velocity 25% lower than the experimental value.

Figures 9 and 10 give a comparison between the numerical and experimental axial velocity profiles at two axial positions, $z = 0.4$ m and $z = 0.65$ m respectively. The

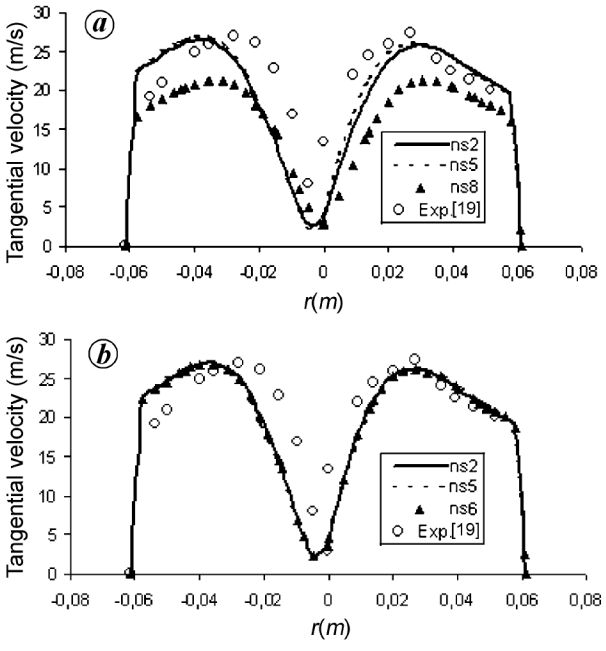

Figure 8 ***a***, ***b***. Comparison between computed tangential velocity profiles and experimental data ($z = 0.4$ m, 0°–180°).

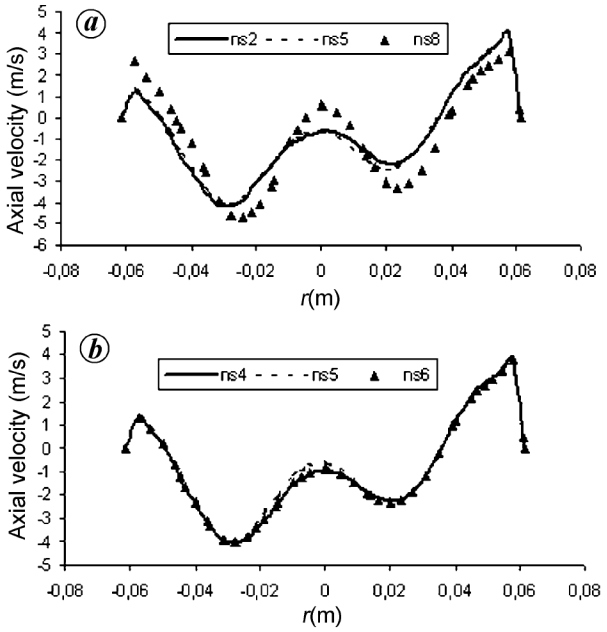

Figure 9 ***a***, ***b***. Comparison of computed axial velocity profiles at $z = 0.4$ m, 0°–180°.

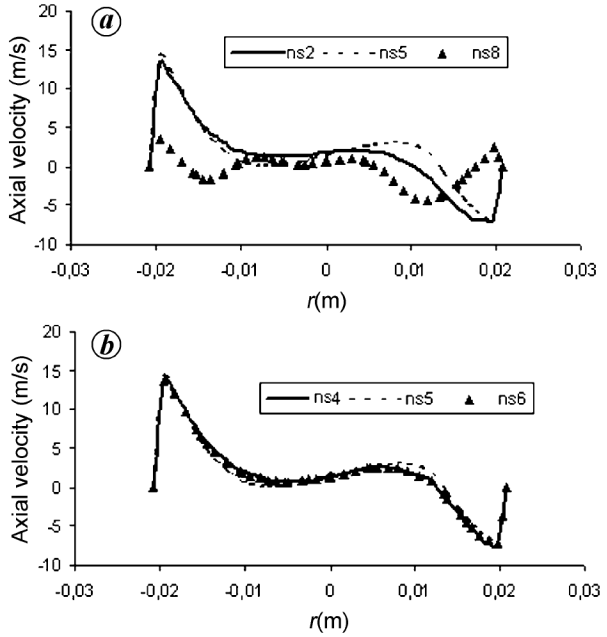

Figure 10 ***a***, ***b***. Comparison of computed axial velocity profiles at $z = 0.65$ m, 0°–180°.

shape of the axial velocity profiles changes considerably and the differences between the numerical solutions became noticeable as the flow spins down towards the cone apex. Near the bottom (z = 0.65 m), ns2 and ns8 give different velocity values.

Conclusion

This study deals with the investigation of turbulence models, numerical schemes and algorithms suitable for highly swirling turbulent flows, as in the case of tangential inlet cyclones. Three turbulence models, namely the RSM, the Standard k–ε and RNG k–ε were tested and the performance of various numerical schemes and algorithms well known in the literature investigated using Fluent CFD code.

It can be concluded from the results that only the RSM turbulence model predicts well the experimental data, due to the strong anisotropy arising from the effects of high swirling and steamline curvature. The Standard k–ε and the RNG k–ε turbulence models present a solid-body rotation rather than the expected combined vortex, and also give an unrealistic distribution of axial velocities. Hence they are unsuitable for highly swirling flows.

Results also show that the pressure interpolation scheme is crucial for accuracy in swirling flows. The presto scheme predicts well the experimental data, whereas the first and second-order interpolation schemes give pressure and velocity values different from experimental data.

Although the numerical schemes used for the momentum equation give similar results, the quick scheme is found to be the best among them; the first and second-order upwind schemes for turbulent quantities also give almost the same results. However, higher order schemes cause convergence problems.

The optimum choice seems to be the second order for turbulence kinetic energy and the first order for Reynolds stresses. The Simplec algorithm for pressure–velocity coupling seems to be advantageous in terms of convergence.

1. Moore, M. E. and Mcfarland, A. R., Performance modelling of single-inlet aerosol sampling cyclones. *Environ. Sci. Technol.*, 1993, **27**, 1842–1848.
2. Kenny, L. C. and Gussman, R. A., Characterisation and modelling of a family of cyclone preseparators. *J. Aero. Sci.*, 1995, **26**, 777–778.
3. Stairmand, C. J., The design and performance of cyclone separators. *Trans. Inst. Chem. Eng.*, 1951, **29**, 356–383.
4. Lapple, C. E., Processes use many collector types. *Chem. Eng.*, 1951, **58**, 144–151.
5. Kim, J. C. and Lee, K. W., Experimental study of particle collection by small cyclones. *Aero. Sci. Technol.*, 1990, **12**, 1003–1015.
6. Köning, C., Büttner, H. and Ebert, F., Designing data for cyclones. *Part. Part. Syst. Charact.*, 1991, **8**, 301–307.
7. Upton, S. L., Mark, D. and Griffiths, W. D., A wind tunnel evaluation of the sampling efficiencies of three bioaerosol samplers. *J. Aero. Sci.*, 1994, **25**, 1493–1501.
8. Shepherd, G. B. and Lapple, C. E., Flow pattern and pressure drop in cyclone dust collectors. *Ind. Eng. Chem.*, 1939, **31**, 1246–1248.
9. Alexander, R. M., Fundamentals of cyclone design and operation. *Proc. Australia Inst. Min. Metall.*, 1949, **152–153**, 203–228.
10. Barth, W., Berechnung und Auslegung von Zyklonabscheiden auf Grund neuerer Untersuchungen. *BWK*, 1956, **8**, 1–9.
11. Barth, W. and Leineweber, L., Evaluation of design of cyclone separators. *Staub. Reinhalt. Luft.*, 1964, **24**, 41–55.
12. Zhu, Y. and Lee, K. W., Experimental study on small cyclones operating at high flow rates. *J. Aero. Sci.*, 1999, **30**, 1303–1315.
13. Avci, A. and Karagoz, I., Effect of flow and geometrical parameters on the collection efficiency in cyclone separators. *J. Aero. Sci.*, 2003, **34**, 937–955.
14. Karagoz, I. and Avci, A., Modelling of the pressure drop in tangential inlet cyclone separators. *Aero. Sci. Technol.*, 2005, **39**, 857–865.
15. Gimbun, J., Chuah, T. G., Fakhru'l-Razi, A. and Choong, T. S. Y., The influence of temperature and inlet velocity on cyclone pressure drop: A CFD study. *Chem. Eng. Prog.*, 2005, **44**, 7–12.
16. Hoekstra, A. J., Derksen, J. J. and Van Den Akker, H. E. A., An experimental and numerical study of turbulent swirling flow in gas cyclones. *Chem. Eng. Sci.*, 1999, **54**, 2055–2065.
17. Ma, L., Ingham, D. B. and Wen, X., Numerical modelling of the fluid and particle penetration through small sampling cyclones. *J. Aero. Sci.*, 2000, **31**, 1097–1119.
18. Ingham, D. B. and Ma, L., Predicting the performance of air cyclones. *Int. J. Energy Res.*, 2002, **26**, 633–652.
19. Gong, A. L. and Wang, L.-Z., Numerical study of gas phase flow in cyclones with the repds. *Aero. Technol.*, 2004, **38**, 506–512.
20. Altmeyer, S., Mathieu, V., Jullemier, S., Contal, P., Midoux, N., Rode, S. and Leclerc, J. P., Comparison of different models of cyclone prediction performance for various operating conditions using a general software. *Chem. Eng. Prog.*, 2004, **43**, 511–522.
21. Patankar, S. V., *Numerical Heat Transfer and Fluid Flow*, Hemisphere Publishing, New York, 1980.
22. Yakhot, V. and Orszag, S. A., Renormalization group analysis of turbulence. I. Basic theory. *J. Sci. Comput.*, 1986, **1**, 1–51.

Received 28 August 2007; revised accepted 20 February 2008